

1 **Revised International Staging System (R-ISS) stage-dependent analysis uncovers oncogenes**  
2 **and potential immunotherapeutic targets in multiple myeloma**

3 Ling Zhong<sup>1,2,3,4,\*</sup>, Xinwei Yuan<sup>5,\*</sup>, Qian Zhang<sup>1,2,3,\*</sup>, Tao Jiang<sup>6,\*</sup>, Huan Li<sup>1</sup>, Jialing Xiao<sup>1</sup>,  
4 Chenglong Li<sup>6</sup>, Lan Luo<sup>7</sup>, Ping Shuai<sup>1</sup>, Liang Wang<sup>1</sup>, Yuping Liu<sup>1</sup>, Man Yu<sup>2</sup>, Yi Shi<sup>1,2,3</sup>, Wei  
5 Zhang<sup>5</sup>, Yunbin Zhang<sup>2,3,#</sup>, Bo Gong<sup>1,2,3,#</sup>

6  
7 <sup>1</sup>Department of Health Management, Sichuan Provincial People's Hospital, University of  
8 Electronic Science and Technology of China, Chengdu, Sichuan, China;

9 <sup>2</sup>The Key Laboratory for Human Disease Gene Study of Sichuan Province and Institute of  
10 Laboratory Medicine, Sichuan Provincial People's Hospital, University of Electronic Science  
11 and Technology of China, Chengdu, Sichuan, China;

12 <sup>3</sup>Research Unit for Blindness Prevention of Chinese Academy of Medical Sciences  
13 (2019RU026), Sichuan Academy of Medical Sciences, Chengdu, Sichuan, China;

14 <sup>4</sup>Natural Products Research Center, Institute of Chengdu Biology, Sichuan Translational  
15 Medicine Hospital, Chinese Academy of Sciences, Chengdu, Sichuan, China

16 <sup>5</sup>Department of Orthopaedics, Sichuan Provincial People's Hospital, University of Electronic  
17 Science and Technology of China, Chengdu, Sichuan, China;

18 <sup>6</sup>Department of hematology, Sichuan Provincial People's Hospital, University of Electronic  
19 Science and Technology of China, Chengdu, Sichuan, China;

20 <sup>7</sup>Chengdu University of Traditional Chinese Medicine, Chengdu, Sichuan, China;

21

22 \*These authors contribute equally to this work.

23

24 #Correspondence should be addressed to:

25

26 Bo Gong, Department of Health Management, Sichuan Provincial People's Hospital,  
27 University of Electronic Science and Technology of China, 32 The First Ring Road West 2,  
28 Chengdu, Sichuan, 610072, China. Email: [gongbo2007@hotmail.com](mailto:gongbo2007@hotmail.com); Phone:

29 86-28-87393375; Fax: 86-28-87393596

30

31 **Abstract**

32 Multiple myeloma (MM), characterized by high intratumour heterogeneity, accounts for ~10%  
33 of all haematologic malignancies. Stratified by the Revised International Staging System  
34 (R-ISS), little is known about R-ISS-related plasma cell (PC) heterogeneity, gene expression  
35 modules in cytotoxic T/NK cells and immunoregulatory ligands and receptors. Herein, we  
36 constructed a single-cell transcriptome atlas of bone marrow in normal and R-ISS-staged MM  
37 patients. Focusing on PCs, we identified and validated a subset of GZMA+ cytotoxic PCs. In  
38 addition, a malignant PC population with high proliferation capability (proliferating PCs) was  
39 associated with unfavourable prognosis and EBV infection in our collected samples.  
40 Ribonucleotide Reductase Regulatory Subunit M2 (RRM2), a specific marker of proliferating  
41 PCs, was shown to induce MM cell line proliferation and serve as a detrimental marker in MM.  
42 Subsequently, three R-ISS-dependent gene modules in cytotoxic CD8+ T and NKT cells were  
43 identified and functionally analysed. Finally, cell-cell communication between neutrophils and  
44 proliferating PCs with cytotoxic CD8+ T and NKT cells was investigated, which identified  
45 intercellular ligand receptors and potential immunotargets such as SIRPA-CD47 and  
46 TIGIT-NECTIN3. Collectively, this study provides an R-ISS-related single-cell MM atlas and  
47 reveals the clinical significance of two PC clusters, as well as potential immunotargets in MM  
48 progression.

49 **Key words** Multiple myeloma; International Staging System (R-ISS); cytotoxic plasma cells;  
50 proliferating plasma cells; EBV infection; SIRPA-CD47; TIGIT-NECTIN3.

51

52

53

## 54 **Introduction**

55 Multiple myeloma (MM) is characterized by uncontrolled proliferation of monoclonal plasma  
56 cells and accounts for ~10% of all haematologic malignancies [1]. The revised International  
57 Staging System (R-ISS) was developed to stratify MM patients into groups I, II and III [2] with  
58 distinct outcomes [3] and treatment response [4] , with or without the assistance of other  
59 clinical parameters [5, 6]. However, the single-cell gene expression signatures in MM R-ISS  
60 stages remain to be explored. Epstein-Barr virus (EBV), the first human tumour virus [7],  
61 causes Burkitt, Hodgkin, and post-transplant B cell lymphomas [8], and is associated with poor  
62 prognosis and clinical characteristics of RISS III in MM patients [9] , although further studies  
63 are needed to uncover the mechanism. In the bone marrow (BM) microenvironment, the  
64 interplay between neoplastic cells and immune microenvironment cells is involved in MM  
65 progression and drug response [10], and single-cell level ligand-receptor interactions remain  
66 unclear. Myeloid cells (such as neutrophils) foster cancer-promoting inflammation, and natural  
67 killer (NK) cells and T lymphocytes mediate protective antitumour responses [11]. With  
68 dramatic advances in immunomodulatory drugs [12-14], monoclonal antibodies [15],  
69 proteasome inhibitors [16], and histone deacetylase inhibitors (HDACis) [17], MM patients still  
70 remain largely incurable [18].

71 Single-cell sequencing (ScRNA-Seq) offers an unprecedented opportunity to study the  
72 heterogeneity of plasma cells and immune microenvironments in cancer. Focusing on plasma  
73 cells, intratumour heterogeneity (ITH) [19], genome evolution [20] and transcriptome  
74 expression signatures [21], resistance pathways and therapeutic targets in relapsed MM [22]  
75 were revealed. Meanwhile, compromised microenvironment immune cells [23] and  
76 transcriptional alterations [24] in MM precursor stages and extramedullary progression were  
77 recently uncovered. Nevertheless, little is known about malignant plasma cell and immune cell  
78 gene expression signatures with respect to the R-ISS stage and their role in EBV-infected MM  
79 at the single-cell level.

80 Herein, we adopted single-cell transcriptome sequencing to investigate the gene expression  
81 profiles in the normal and R-ISS stage I, II and III groups. First, we examined the heterogeneity  
82 of plasma cells and validated the function and clinical significance of two rare plasma cell  
83 populations. The function and clinical significance of proliferating PCs and the hub gene RRM2  
84 were validated in other cohorts, cell lines and collected samples. Subsequently, gene  
85 expression modules underlying two T cell clusters with decreased proportions along with MM  
86 R-ISS stage were investigated. Finally, cell-cell communication was analysed to interpret the  
87 tumour cell-cytotoxic T cell and cytotoxic T cell-neutrophil interactions in MM. Collectively, the  
88 results of this study provide an R-ISS-related single-cell MM atlas and reveal the clinical  
89 significance of two PC clusters, as well as potential immunotargets in MM progression.

90

91

92

## 93 Results

### 94 *Single-cell transcriptome atlas of R-ISS-staged multiple myeloma*

95 To explore the intratumoural heterogeneity of R-ISS stage-classified multiple myeloma, 11  
96 bone marrow samples from 2 healthy donors (healthy control, HC), 2 R-ISS I, 2 R-ISS II and 5  
97 R-ISS III stage MM patients were subjected to single-cell suspension parathion and  
98 transcriptome sequencing (**Fig 1A**). After low-quality cell filtering and quality control, 103,043  
99 single-cell expression matrixes were acquired. Subsequent dimensional reduction generated  
100 21 clusters (**Fig 1B**). Most clusters existed in all four groups (**Fig 1C**), showing a batch-effect  
101 removal basis for the following analysis. Then, based on the cell type markers, six general cell  
102 types were identified, including plasma cells, B cells, myeloid cells, CD4+ T cells, CD8+ T cells  
103 and immature red cells (**Fig 1D-1E**). The proportions of 21 cell clusters in all groups are shown  
104 in **Fig 1F**.

### 105 *Functional identification of a rare cytotoxic NKG7+GZMA+plasma cell population in MM*

106 Intraclonal heterogeneity in plasma cells is emerging as a vital modulator in MM progression  
107 [25], drug sensitivity and therapeutic response [26]. In **Fig 1D**, 7 clusters (3, 8, 10, 14, 15, 18  
108 and 21) specifically expressing high levels of CD138 were classified into plasma cells. Then,  
109 specific markers in each plasma cell cluster were calculated. All 7 clusters showed abundant  
110 expression of ribosomal proteins such as RPS2 and RPL26, which corresponds to the  
111 antibody-producing function of plasma cells. Based on the expression of specific markers, all 7  
112 clusters were generally classified into two groups, group 1: C3, C8, C10, C21 and group 2:  
113 C14, C15, and C18, consistent with the layout of these clusters in Fig 1B. Comparatively,  
114 increased expression of CCL3, NES and S100A8, DEFA3, S100A9, S100A12 and CAMP was  
115 observed in group 1 and group 2, respectively (**Fig 2A**). Notably, C21 exhibits a marker  
116 expression signature distinct from other clusters in the two groups. The cytotoxic genes NKG7,  
117 GZMA, and GNLY and the chemokines CCL5 and CCL4 were exclusively expressed in C21  
118 cells and were defined as “cytotoxic plasma cells”. Maria et al. reported that plasma cells  
119 producing granzyme B (GZMB) showed cancer cell cytotoxic activities [27], but studies of

120 cytotoxic plasma cells in MM remain limited. The existence of cytotoxic plasma cells prompted  
121 us to investigate their existence and clinical relevance in MM. Considering that C21 accounts  
122 for a rare population (average 2.04%, ranging from 0%-10.00%) in all plasma cells (**Fig 2B**),  
123 we first validated its existence with another MM single-cell dataset. In studies focusing on  
124 plasma cell heterogeneity of symptomatic and asymptomatic myeloma (dataset GSE117156)  
125 [19], 4 markers of C21 were indeed exclusively expressed in one plasma cell cluster (cluster 9  
126 in GSE117156, c9) (**Fig 2C-2D**). Of all 42 samples, the cell proportion varied from 0% to  
127 30.95% of all plasma cells, with an average percentage of 4.28%, and 32 samples (76.19%)  
128 showed a percentage <5% (**Fig 2E**). In summary, we characterized a rare NKG7+GZMA+  
129 plasma cell population with cytotoxic activity, which may provide a novel perspective for the  
130 cytotherapy of MM.

### 131 *Clinical significance of a malignant plasma cell population with high proliferation potential*

132 Copy number is a common feature of MM, which usually interferes with cell cycle checkpoints  
133 to prompt accelerated proliferation [28]. To explore the oncogenic gene expression and signal  
134 transduction of plasma clusters in MM, we first conducted InferCNV to delineate the copy  
135 number variation (CNV) signals of all clusters. As shown in **Fig 3A**, strong copy number signal  
136 alterations were observed in clusters 3, 8 and 10, indicating their malignant features as tumour  
137 cells. Consistent with bulk genomic sequencing results, gain/amplification and deletion signals  
138 were mainly located on chromosomes 1, 8 and 2, 3 and 21 [29, 30]. Then we calculated the  
139 cell cycle of plasma cell clusters, and distinguished from other clusters, plasma cells in clusters  
140 8 (C8) and 10 (C10) were presumably enriched in G2/M stage (**Fig 3B**). Expression of cell  
141 proliferation, cell cycle related oncogenic markers MKI67, TOP2A and CDK1 also showed  
142 similar pattern with overall cell cycle, suggesting a high proliferation potential of C8 and C10 in  
143 MM (**Fig 3B**). In R-ISS staged samples, C8 showed remarkably higher proportion in III stage  
144 group (**Fig1F**), and C10 were only detected in R-ISS I and III groups. Similar to C21, the  
145 existence of C10 was also validated in dataset GSE117156 (**Fig 3C**). Then GSEA analysis  
146 was conducted to dig into the signaling transduction in all 3 malignant clusters C3, C8 and C10.

147 As shown in **Fig 3D**, unfolded protein response, E2F targets and epithelial mesenchymal  
148 transition were the most enriched hallmark pathways in C3, C8 and C10, indicating their  
149 functional distinct roles in MM [31-34]. Finally, we applied PRECOG [35] to delineate the gene  
150 expression specificity in clusters and the prognostic score in MM with bulk sequencing  
151 GSE6477 metadata. As a result, most genes with high specificity in C10 also showed elevated  
152 prognostic Z scores, such as GGH (z-score=6.1), GINS2 (z-score=4.5), PRKDC (z-score=6.1),  
153 MCM3 (z-score=4.4), SHCBP1 (z-score=4.7), CHEK1 (z-score=3.9) and PHF19 (z-score=5.5)  
154 (**Fig 3E**). Therefore, we focused on C10, a malignant plasma cell population with high  
155 proliferation potential and unfavourable prognostic significance, and investigated its clinical  
156 relevance and potential therapeutic targets in MM.

157 Next, we discovered 75 significantly up-regulated genes in the MM (UGM) dataset of  
158 GSE6477 as compared with normal samples (**Fig 4A-4B**). The top 150 specific genes in C10  
159 were compared with 75 UGMs, and 7 genes (CADM1, HIST1H1C, CD48, RRM2, PPIB, LDHB  
160 and HINT1) were acquired (**Fig 4C**). The expression of 7 UGMs is shown with the R-ISS stage  
161 in **Fig 4D**. We calculated a 7-gene signature score and analyzed the relevance of the score  
162 with respect to clinical parameters (**Fig 4E**). Next, the prognostic significance of these 7 genes  
163 was analyzed. RRM2 and HINT1 showed good performance as unfavorable markers, with  
164 HR=2.3 (95% CI=1.4-3.6, p-value<0.000402) and HR=1.9 (95% CI=1.2-2.9, p-value=  
165 0.005496), respectively (**Fig 4F**). Then, the expression of RRM2 and HINT1 was examined in  
166 MM patients and MM.1S and U266 MM cell lines. Consistently, significantly increased  
167 expression of RRM2 and HINT1 was observed in both clinical MM R-ISS III samples (**Fig 4G**)  
168 and MM cell lines (MM.1S and U266) (**Fig 4H**). Next, the functions of RRM2 and HINT1 in the  
169 MM cell line U266 were studied. RRM2 and HINT1 silencing reduced the proliferation of U266  
170 cells, respectively (**Fig 4I**).

171 Finally, we calculated the differentially expressed genes (DEGs) with fold change  $\geq 2$  or  $\leq$   
172  $0.5$  and adjusted p value  $< 0.05$  in C10 by comparing R-ISS stages I and III. All 150 DEGs  
173 were acquired. Then, we constructed a functional analysis of these 150 DEGs. As shown in

174 **Fig 5A**, 5 functional gene modules were identified: a) ribosome, b) protein processing in  
175 endoplasmic reticulum, c) oxidative phosphorylation, d) proteasome, and e) Epstein-Barr virus  
176 infection. It is not surprising that protein and energy metabolism-related modules, such as  
177 ribosomes in protein translation, protein processing in the endoplasmic reticulum and  
178 proteasomes in protein degradation and oxidative phosphorylation, are enriched, which  
179 provides a synthetic basis for MM progression. Intriguingly, 10 genes (MDM2, CCND2, CDK6,  
180 STAT3, HLA-F, HLA-B, HLA-C, HLA-E, JUN, PSMC1) involved in Epstein-Barr virus infection  
181 and sub-modules of viral carcinogenesis attracted our attention. We then validated the  
182 expression of MKI67 and PCNA, two proliferating markers in MM patients. Indeed, significantly  
183 elevated expression of MKI67 and PCNA was observed in EBV-positive (EBV+) MM patients  
184 compared with EBV-negative (EBV-) MM patients (**Fig 5B-5C**). Finally, potential therapeutic  
185 drugs were analysed based on pathways in C10, and alsterpaullone (cyclin-dependent kinase  
186 inhibitor) [36], orlistat (anti-obesity drug) [37], moxonidine (a selective imidazoline/alpha2  
187 adrenergic receptor agonist)[38], nalidixic acid (topoisomerase II inhibitors) [39] and  
188 LY-294002 (PI3K/AKT inhibitor) [40] were proposed as C10-targeting pharmaceuticals in MM  
189 (**Fig 5D**).

190 ***R-ISS stage-dependent expression analysis highlights functional modules underlying cytotoxic***

191 ***T cell decreases***

192 Accumulating evidence demonstrates that the compromised tumour immune  
193 microenvironment (TIME) contributes to MM progression [41], and therapeutic agents  
194 targeting the TIME have emerged as promising avenues [13, 42]. As one of the major cytotoxic  
195 immune cell types, T cell dysfunction is well acknowledged [43] and immunotherapies such as  
196 chimaeric antigen receptor (CAR) T cells [44] and immune checkpoint inhibitors [45] have  
197 entered clinical trials. Here, we propose a hypothesis that the proportions of certain cytotoxic T  
198 cell populations decrease with MM progression: we stratified them according to the R-ISS  
199 system and attempted to identify the functional genes within.

200 First, re-clustering of T cells generated 21 clusters (**Fig 6A**), T1 to T21, belonging to CD4+ T



201 cells, CD8<sup>+</sup> T cells, NK cells and NKT cells (**Fig 6B and 6D**). No biased distribution was  
202 observed in 11 samples (**Fig 6C**). The percentages of T1 to T21 in MM versus healthy controls  
203 and MM R-ISS I to III are presented in **Fig 6E and Fig 6F**, respectively. It is worth noting that 2  
204 clusters conform to the hypothesis of decreased percentage along with R-ISS stages: T2 and  
205 T10. T2 was marked by high expression of CD8A and no expression of NKG7 and was  
206 identified as CD8<sup>+</sup> T cells. T10 cells express both CD8A and NKG7 and were defined as NKT  
207 cells. We concentrate on T2 and T10 in the following work.

208 To identify R-ISS-dependent gene modules in T2 and T10, the R package MFUZZ [46] was  
209 applied. As a result, in T2 CD8<sup>+</sup> T cells, 12 gene modules with distinct expression patterns  
210 were generated, and module 5 (gradually increased expression with R-ISS stage) and module  
211 3 (gradually decreased expression with R-ISS stage) were chosen for subsequent analysis  
212 (**Fig 7A-7B**). As expected, genes in module 5 were functionally related to antigen processing  
213 and presentation, T cell activation and haemopoiesis (**Fig 7D**). Surprisingly, genes in module 3  
214 were involved in neutrophil activation (**Fig 7E**), which prompted us to examine neutrophils in  
215 MM. Significantly, the proportion of activated neutrophils characterized by CXCR2 expression  
216 [47-49] (C5 in Fig 1B) decreased with R-ISS stage (C5 in Fig 1F). Hence, we speculated that  
217 the decrease in activated neutrophils among MM R-ISS stages may be attributed to decreased  
218 expression of module 3 genes such as CXCR1 [50], ADAM10 [51] and CD47 [52] in T2  
219 cytotoxic cells. For T10, genes in module 1 showed stable expression in healthy controls,  
220 R-ISS I and II, while dramatic increases in R-ISS III were observed (**Fig 7C**). Subsequent  
221 ClueGo results (**Fig 7F**) revealed genes involved in T cell/lymphocyte differentiation (IL2RA,  
222 CD74, CD86, IL7 and RIPK2), adaptive immune response to tumour cells (NECTIN2, IL12A,  
223 NRG1 and HSPD1) and nucleotide-binding oligomerization domain (NOD1)-containing  
224 signalling pathways (HSPA1A, BIRC3, IRAK1, HSP90AA1 and HSPA1B).

225 *Ligand-receptor pairs and potential immunotherapeutic targets in CD8<sup>+</sup> T-neutrophil and*  
226 *CD8<sup>+</sup> T/NKT-plasma cell communication*

227 Finally, we employed CellPhoneDB [53] to interrogate ligand-receptor pairs between T2 CD8<sup>+</sup>

228 T cell-C5 myeloid neutrophils (**Fig 8A**) and T2 CD8+ T cell/T10 NKT cell-C10 proliferating  
229 plasma cells (**Fig 8C**). As shown in **Fig 8B**, 19 ligand-receptor pairs were proposed as T2  
230 CD8+ T cells to C5 neutrophil modulators, such as chemokine ligand receptors  
231 CCL5/CCL3/CCL4L2-CCR1, IFN-IFN receptors (IFNRs), CD99-PILPA and CD52-SIGLEC10.  
232 On the other hand, 21 ligand-receptor pairs were proposed as C5 neutrophils to T2 CD8+ T  
233 cell modulators, such as chemokine ligand receptors ICAM1/3-SPN/ITGAL, CD55-ADGRE5,  
234 SEMA4A-PLXND1, SIRPA-CD44/CD47, IL1B-ADRB2 and CD48-CD244. For T2 CD8+ T  
235 cell/T10 NKT cell communication with C10 proliferating plasma cells, common ligand-receptor  
236 pairs such as TIGIT-NECTIN3, ADRB2\_VEGFB, CD74\_COPA, and CD74\_MIF were identified.  
237 On the other hand, common ligand-receptor pairs such as MDK-SORL1, MIF-TNFRSF14,  
238 FAM3C-CLEC2D, and ICAM1-ITGAL were also enriched (**Fig 8D**). Altogether, we found that  
239 the ligand-receptor pairs between CD8+ T cells/T10 NKT cells, plasma cells and neutrophils  
240 suggested a complex communication network in the MM TIME, which could provide clues for  
241 MM progression and therapy.

242 **Discussion**

243 Multiple myeloma (MM) is characterized by uncontrolled proliferation of monoclonal plasma  
244 cells, and the R-ISS System was developed to stratify MM patients into groups I, II and III [2]  
245 with distinct outcomes [3] and treatment response [4]. This study identified malignant plasma  
246 cells with potent proliferation ability. Moreover, RRM2 and HINT1 with unfavourable prognostic  
247 significance in MM were also characterized. RRM2, regulated in a cyclin F-dependent fashion  
248 [54], encodes one of two nonidentical subunits for ribonucleotide reductase and is well studied  
249 as an oncogene and poor prognostic marker in multiple solid cancer types [55-57]. Meanwhile,  
250 RRM2 inhibition induced synergy with gemcitabine in lymphoma [58] and WEE1 inhibitor in  
251 H3K36me3-deficient cancers [59]. In MM, RRM2 knockdown alone inhibits MM cell  
252 proliferation and induces apoptosis via the Wnt/ $\beta$ -catenin signalling pathway [60]. In contrast,  
253 histidine triad nucleotide binding protein 1 (HINT1) encodes a protein that hydrolyses purine  
254 nucleotide phosphoramidate substrates and is mostly believed to be a tumour suppressor in  
255 multiple cancer types [61-63]. Another finding in malignant plasma cells is the involvement of  
256 genes (MDM2, CCND2, CDK6, STAT3, HLA-F, HLA-B, HLA-C, HLA-E, JUN, PSMC1) in  
257 Epstein-Barr virus (EBV) infection and viral carcinogenesis [64-67]. Further in-depth studies of  
258 their roles in EBV infection and plasma cell proliferation are needed in the future.

259 Intriguingly, we also found a rare plasma cell proportion with cytotoxic activities (high  
260 expression of NKG7 and GZMA) in the BM microenvironment of MM patients for the first time.  
261 T cells and NK cells are the two main types of cytotoxic immune cells in previous studies.  
262 Coincidentally, plasma/B cells producing granzyme B (GZMB) also possess cytotoxic activities  
263 and induce HCT-116 cell death [27]. To be cautious, we first validated the existence of these  
264 cytotoxic NKG7/GZMA<sup>+</sup> plasma cells in another single-cell dataset. If possible, we collected  
265 more MM samples and applied FACS to verify its existence, although the proportion in all  
266 plasma cells was small. Furthermore, to explore the function of NKG7/GZMA<sup>+</sup> plasma cells, in  
267 vitro cytotoxicity assays should be conducted to study the function of NKG7/GZMA<sup>+</sup> plasma  
268 cells in inducing cell death in MM. Altogether, this discovery offers an alternative option for the

269 cytotherapy of MM.

270 In addition, we also identified multiple immunotherapeutic targets in MM. CD24 is a highly  
271 expressed, anti-phagocytic signal in several cancers and demonstrates therapeutic potential  
272 for CD24 blockade in cancer immunotherapy [68]. ICAM-1 antibodies showed potent  
273 anti-myeloma activity in multiple studies [69] [70] [71]. CD44 mediates resistance to  
274 lenalidomide in multiple myeloma [72], and CD44-targeted T cells mediate potent anti-tumour  
275 effects against multiple myeloma [73]. CD47 on macrophages represents a "do-not-eat-me"  
276 immune checkpoint [74]. CD48 was expressed on more than 90% of MM plasma cells, and  
277 administration of the anti-CD48 mAb significantly inhibited MM growth [75]. CD74 is  
278 predominantly expressed in malignant plasma cells, and anti-CD74 mAbs internalize very  
279 rapidly and have shown efficacy in B-lymphoma models [76] [77]. MIF is an important player  
280 and a novel therapeutic target in MM. Inhibiting MIF activity will sensitize MM cells to  
281 chemotherapy [78]. MIF plays a crucial role in MM sensitivity to PIs and suggests that targeting  
282 MIF may be a promising strategy to (re)sensitize MM to treatment [79]. T-cell immunoglobulin  
283 and ITIM domains (TIGIT) are other immune checkpoint receptors known to negatively  
284 regulate T-cell functions. MM progression was associated with high levels of TIGIT expression  
285 on CD8 T cells. TIGIT CD8 T cells from MM patients exhibited a dysfunctional phenotype  
286 characterized by decreased proliferation and inability to produce cytokines in response to  
287 anti-CD3/CD28/CD2 or myeloma antigen stimulation. TIGIT immune checkpoint blockade  
288 restores CD8 T-cell immunity against multiple myeloma [80]. Nectin-2 expression on malignant  
289 plasma cells is associated with better response to TIGIT blockade in multiple myeloma [81].  
290 Myeloma escape after stem cell transplantation is a consequence of T-cell exhaustion and is  
291 prevented by TIGIT blockade [82].

292 In conclusion, we constructed a single-cell transcriptome atlas of bone marrow in normal and  
293 R-ISS-staged MM patients. Focusing on PCs, we identified and validated the existence of  
294 GZMA+ cytotoxic PCs. In addition, a malignant PC population with high proliferation capability  
295 (proliferating PCs) was clinically associated with EBV infection and unfavourable prognosis.

296 Ribonucleotide Reductase Regulatory Subunit M2 (RRM2), a specific marker of proliferating  
297 PCs, was shown to induce MM cell line proliferation and serve as a detrimental marker in MM.  
298 Subsequently, three R-ISS-dependent gene modules in cytotoxic CD8+ T and NKT cells were  
299 identified and functionally analysed. Finally, cell-cell communication between neutrophils and  
300 proliferating PCs with cytotoxic CD8+ T and NKT cells was investigated, which identified  
301 intercellular ligand receptors and potential immunotargets such as SIRPA-CD47 and  
302 TIGIT-NECTIN3. Collectively, the results of this study provide an R-ISS-related single-cell MM  
303 atlas and reveal the clinical significance of two PC clusters, as well as potential immunotargets  
304 in MM progression.

### 305 **Acknowledgements**

306 We thank all the patients and their families for participating in this study. The present study  
307 was supported by the grant from the National Natural Science Foundation of China (82002212,  
308 81870683, 82070928), the Science & Technology Department of Sichuan Province (19YJ0593,  
309 2020ZYD035, 2020YJ0460, and 2020JDTD0028), Department of Sichuan Provincial Health  
310 (19PJ117), the Sichuan Provincial People's Hospital (2018LY03), the Chengdu Science and  
311 Technology Bureau (2019-YF05-00572-SN), the China Postdoctoral Science Foundation  
312 Grant (2019M663567), the foundation of Basic scientific research in Central Universities of  
313 University of Electronic Science and technology (ZYGX2020J024).

314

### 315 **Authors' contributions**

316 Bo Gong, Ling Zhong and Yunbin Zhang conceived the idea. Ling Zhong, Xinwei Yuan,  
317 JiangTao, Huan Li, and Jialing Xiao collected the specimen and prepared single-cell  
318 suspension for sequencing. Ling Zhong, Qian Zhang, Xinwei Yuan, Ping Shuai, Liang Wang,  
319 Yuping Liu, Man Yu and Yi Shi finished the bioinformatics analysis. Lan Luo and Chenglong Li  
320 accomplished the flow cytometry. Jialing Xiao finished immunofluorescence staining. Ping  
321 Shuai, and Yuping Liu finished the qPCR. Ling Zhong, Bo Gong, and Yunbin Zhang wrote the  
322 manuscript. All authors reviewed and approved the manuscript.

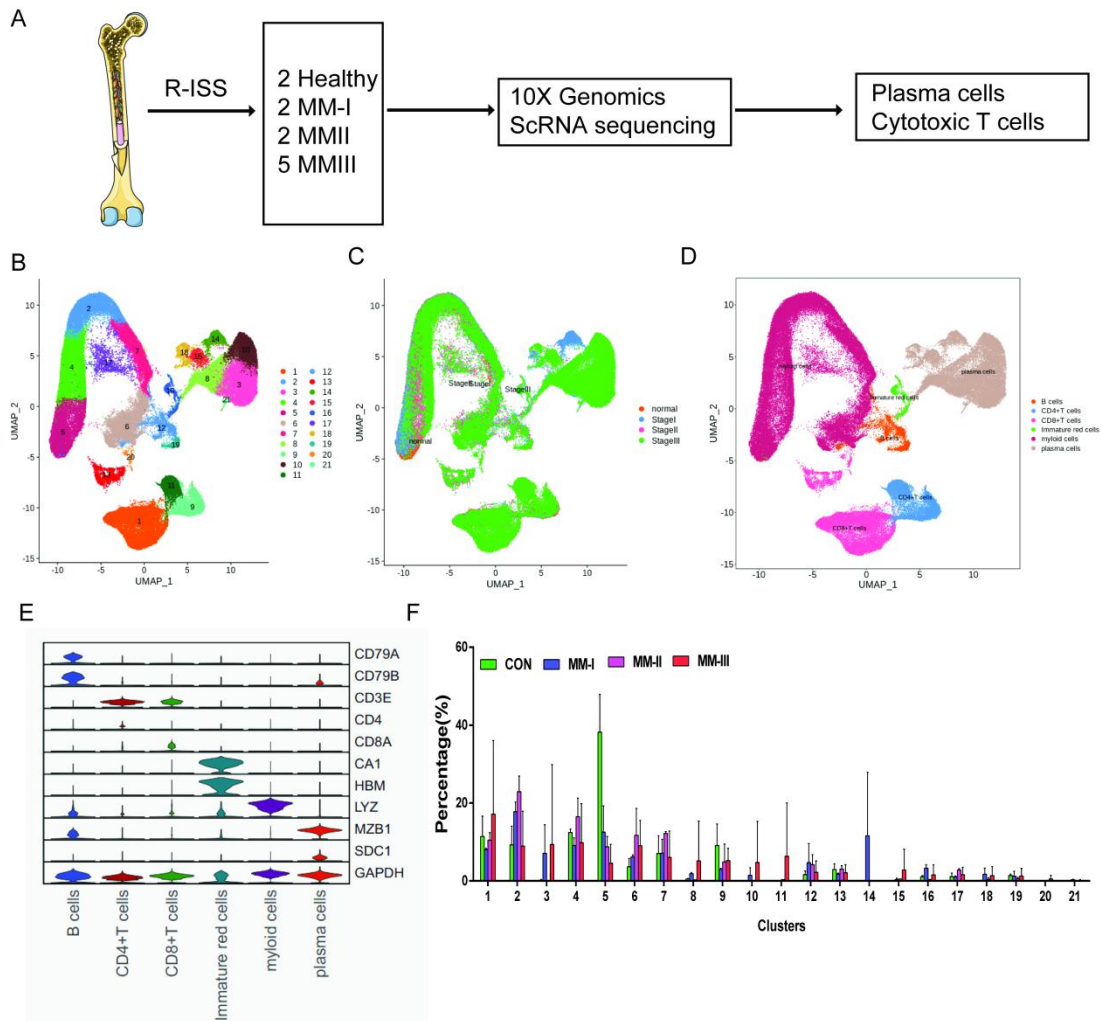
323

### 324 **Data availability**

325 Sequencing data have been deposited in GEO under accession code GSE176131.

326

327 **Figure legends**



328

329 **Figure1. Single cell transcriptome atlas of Multiple myeloma (MM) with R-ISS staging.**

330 A) Schematic illustration of workflow in this study;

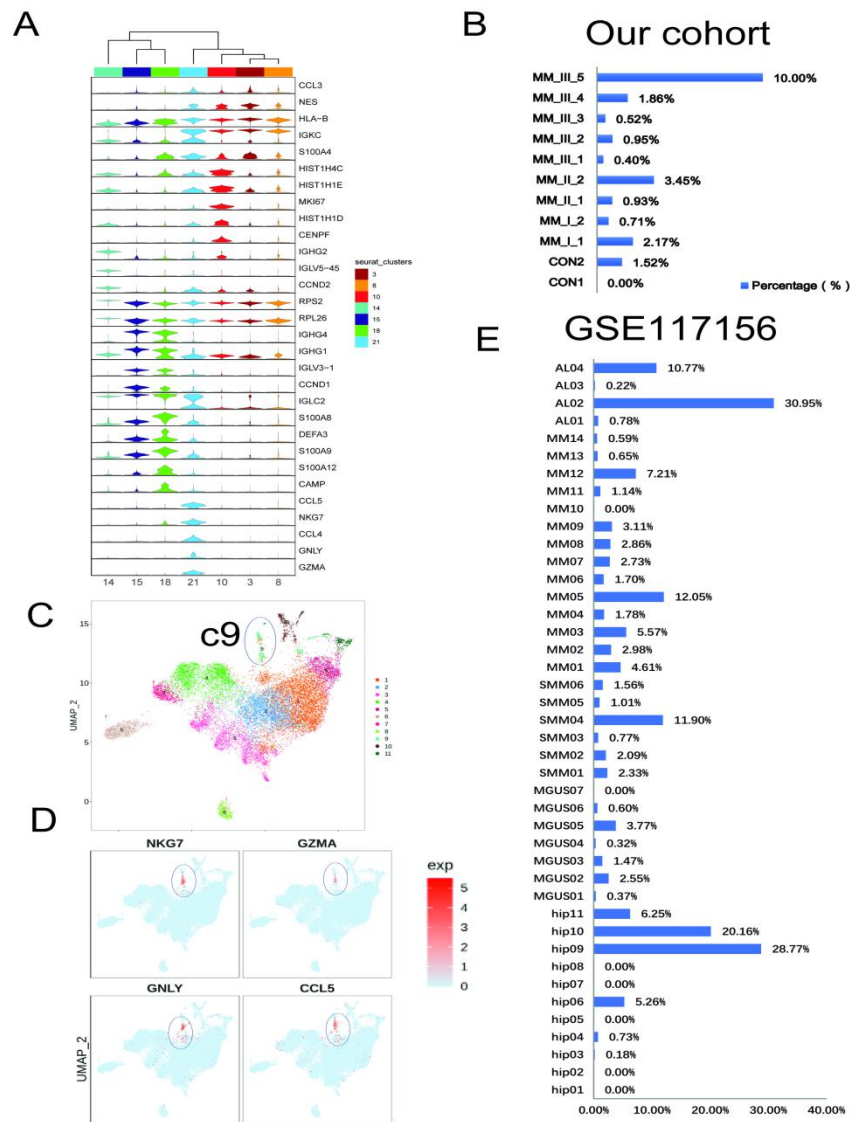
331 B) Dimension reduction of cells, and 21 clusters were acquired, shown with UMAP;

332 C) UMAP showing the distribution of sample groups of Normal, R-ISS I to III;

333 Based on expression signature of canonical markers, six general cell types were identified.

334 UMAP of cell type in were shown D), and violin plot of cell type markers in E);

335 F) Proportion of cell clusters in normal and MM RISS groups;



336

337 **Figure2. Identification of a rare cytotoxic NKG7+GZMA+plasma cell population in MM**

338 A) The heterogeneity of plasma cells (CD138+) was transcriptionally analyzed, and genes  
339 specifically expressed in 7 plasma cell clusters were calculated.

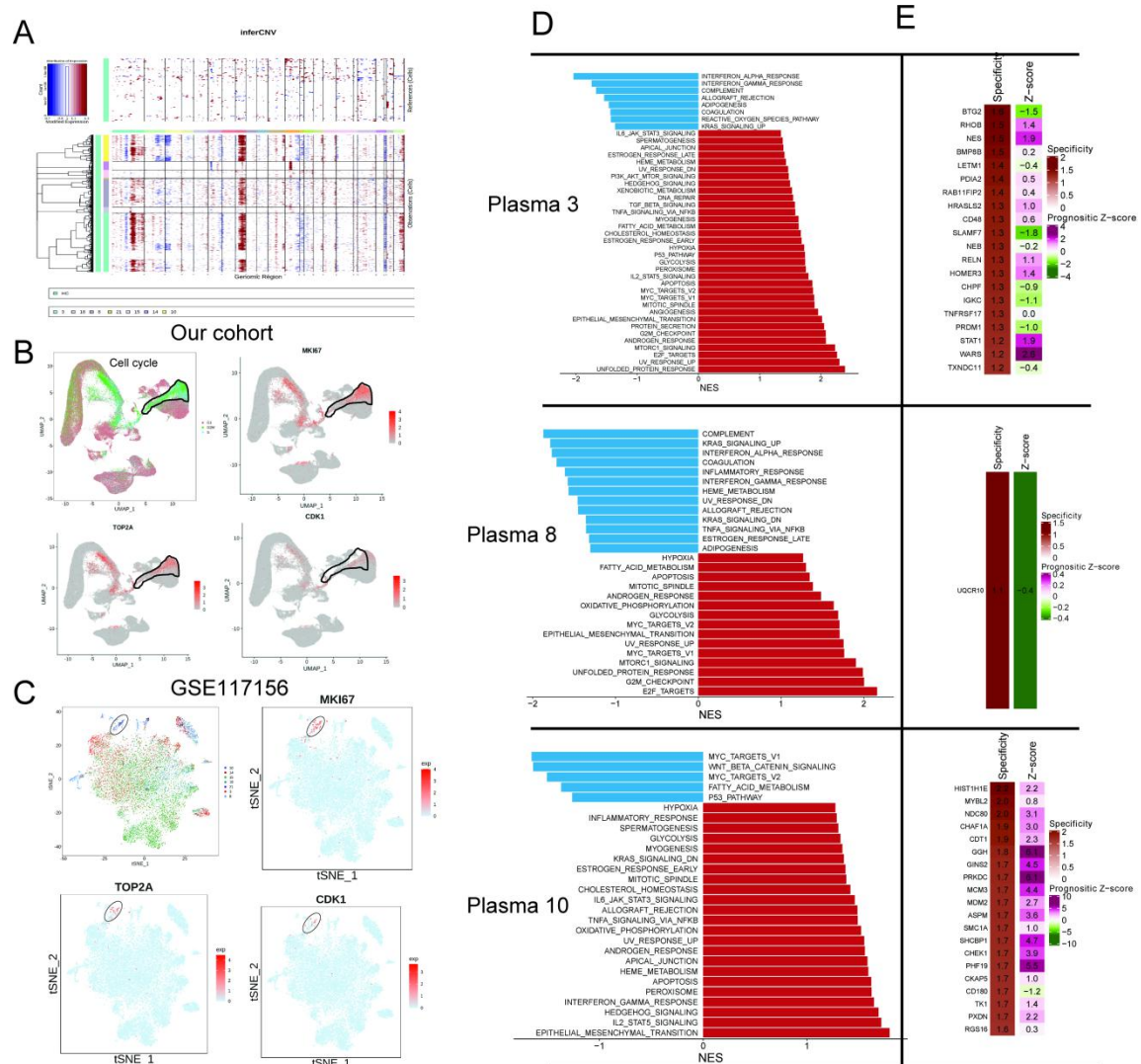
340 B) In our cohort, C21 accounts for a rare population (average 2.04%, ranges from 0%-10.00%)  
341 in all plasma cells;

342 C) C21 corresponds to c9 in another MM plasma dataset of GSE117156;

343 D) C21 specifically highly expresses cytotoxic markers like NKG7, GZMA, GNLY and CCL5;

344 E) The cell fraction of c9 in another MM plasma dataset of GSE117156.

345



346

347 **Figure3. Identification of a malignant and risky plasma cell cluster with proliferation activity.**

348 A) To identify malignant plasma cells, inferCNV was applied to obtain the CNV signals in all 7  
 349 plasma cell clusters.

350 B) Cell cycle distribution was analyzed, and shown with UMAP. UMAP of 3 proliferation  
 351 markers of MKI67, TOP2A and CDK1 were also shown.

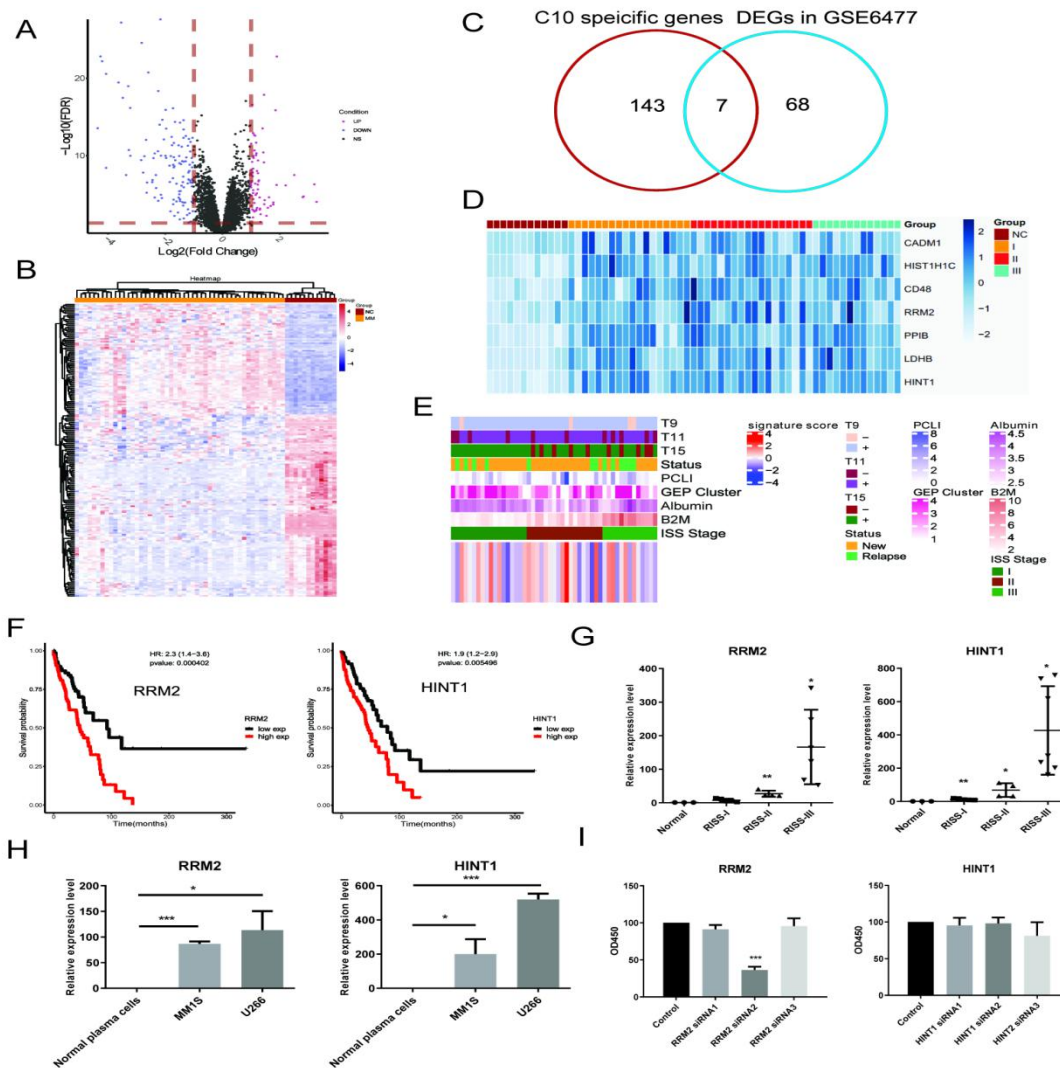
352 C) UMAP of 3 proliferation markers of MKI67, TOP2A and CDK1 in GSE117156.

353 D) GSEA hallmarks analysis were conducted, and significant enriched pathways of clusters  
 354 3,8 and 10 were shown.

355 E) Precog was applied to infer the genes with specificity and prognostic Z-score in external

356 MM gene expression data GSE6647;





357

358 **Figure 4. Bulk sequencing validation highlights C10 specific genes RRM2 and HINT1 as novel**  
 359 **prognostic markers in MM.**

360 All 75 significant deregulated genes in GSE6647 dataset MM group was acquired, and shown  
 361 with A) volcano plot and B) heatmap;

362 C ) Top 150 specific genes with markers potential was compared with 75 DEGs in MM dataset  
 363 of GSE6647, and 7 genes were acquired and named as deregulated proliferating marker  
 364 genes in MM (DPMGs);

365 D) The expression of 7 DPMGs in normal and RISS-I to III stages were shown, and all 7  
 366 DPMGs were up-regulated in MM, especially in RISS-III stage;

367 E) Clinical parameters of MM samples with 7-gene signature score.

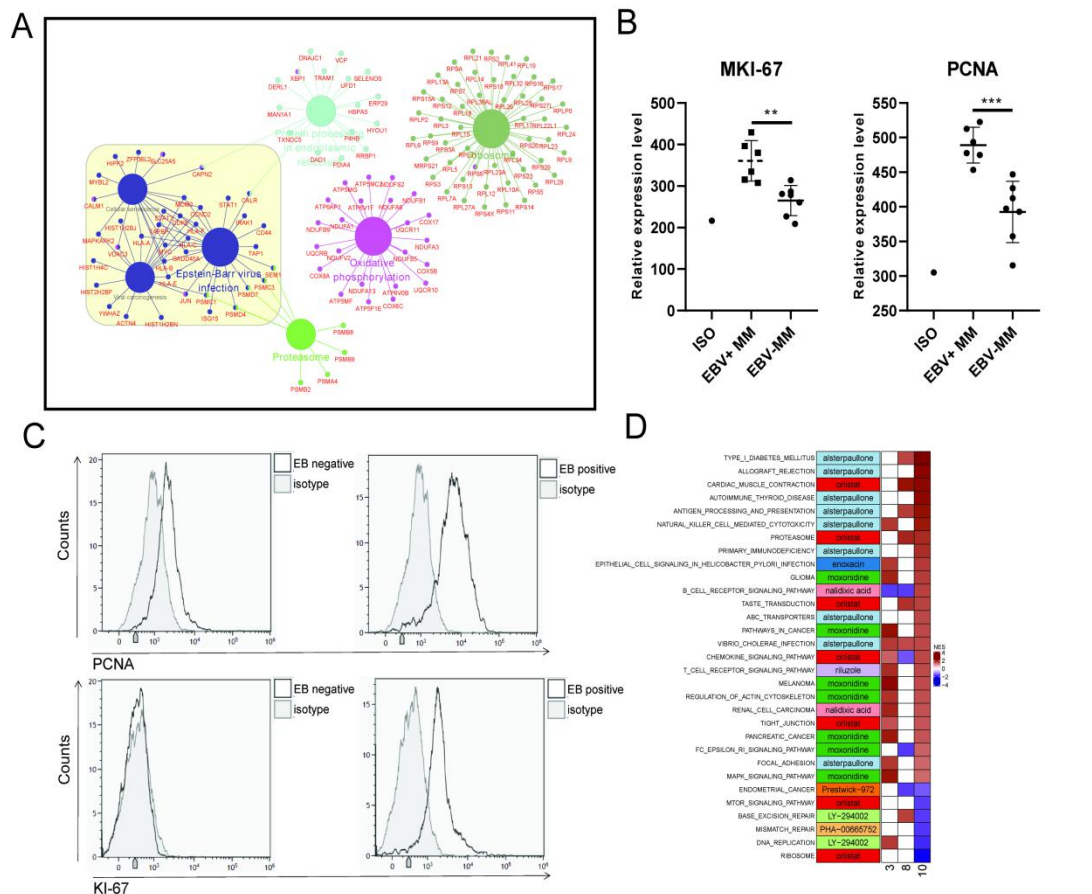
368 F) Two DPMGs, RRM2 and HINT1, exhibited good performance as unfavorable prognostic  
 369 markers in MM patients.

370 G) Relative quantification of RRM2 and HINT1 by qRT-PCR in healthy and RISS stratified MM  
 371 patient BM samples;

372 H) Relative quantification of RRM2 and HINT1 by qRT-PCR in normal plasma cells and MM1S  
 373 and U266 cell lines;

374 I) Proliferation phenotype of RRM2 and HINT1 silencing in MM cell line U266.

375 Values represent the means of three experiments  $\pm$  SD; \*  $p < 0.05$ , \*\*  $p < 0.01$ , versus  
 376 untreated control.



377

378 **Figure 5. Proliferating plasma cells were increased in EBV positive MM patients.**

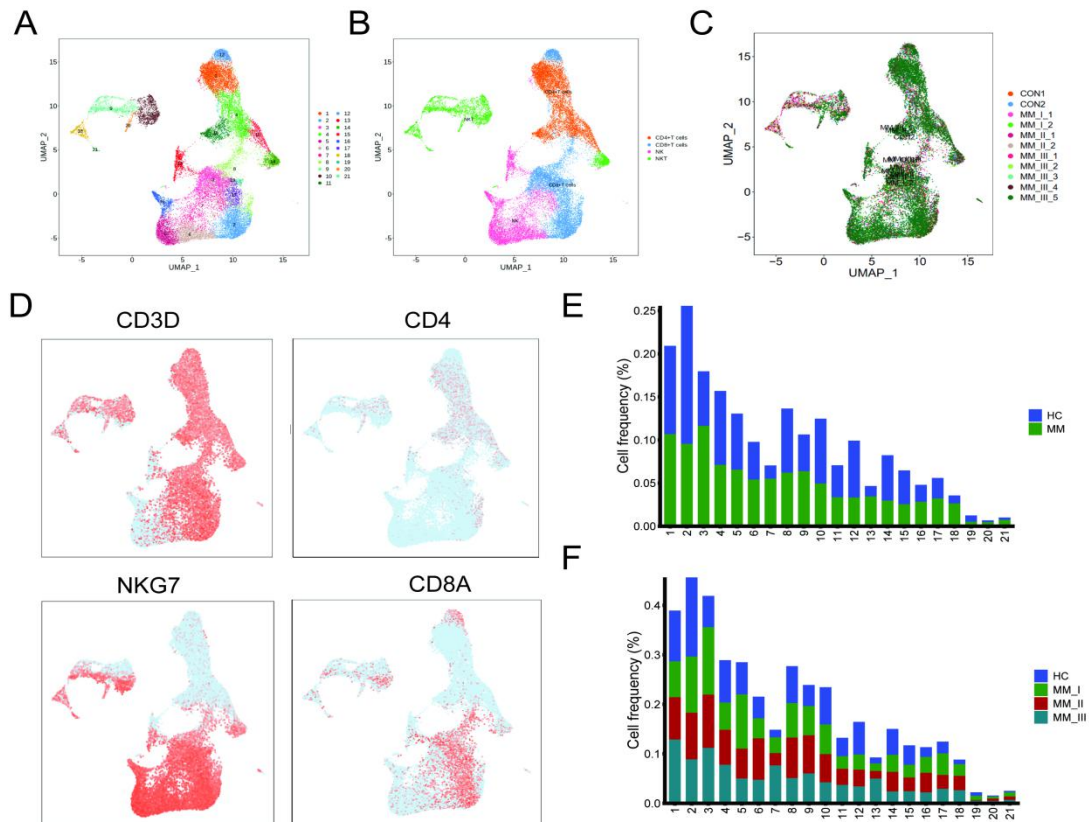
379 A) DEGs in MM RISS III stage with I stage were obtained and conferred to functional  
 380 analysis;

381 B) Relative Expression of MKI-67 and PCNA in EBV positive and EBV negative MM patients

382 BM samples;

383 C) Representative FACS peaks of MKI-67 and PCNA in EBV positive and EBV negative MM  
384 patients;

385 D ) Based on pathways enriched in plasma clusters 3, 8 and 10, potential drug candidates  
386 were acquired, and shown with heatmap;



387

388 **Figure6. T cell population analysis suggested Stage-dependent CD8+T and NKT cell clusters**  
389 **depletion in MM.**

390 A) T cells and NK cells were re-clustered, and 21 clusters were acquired;

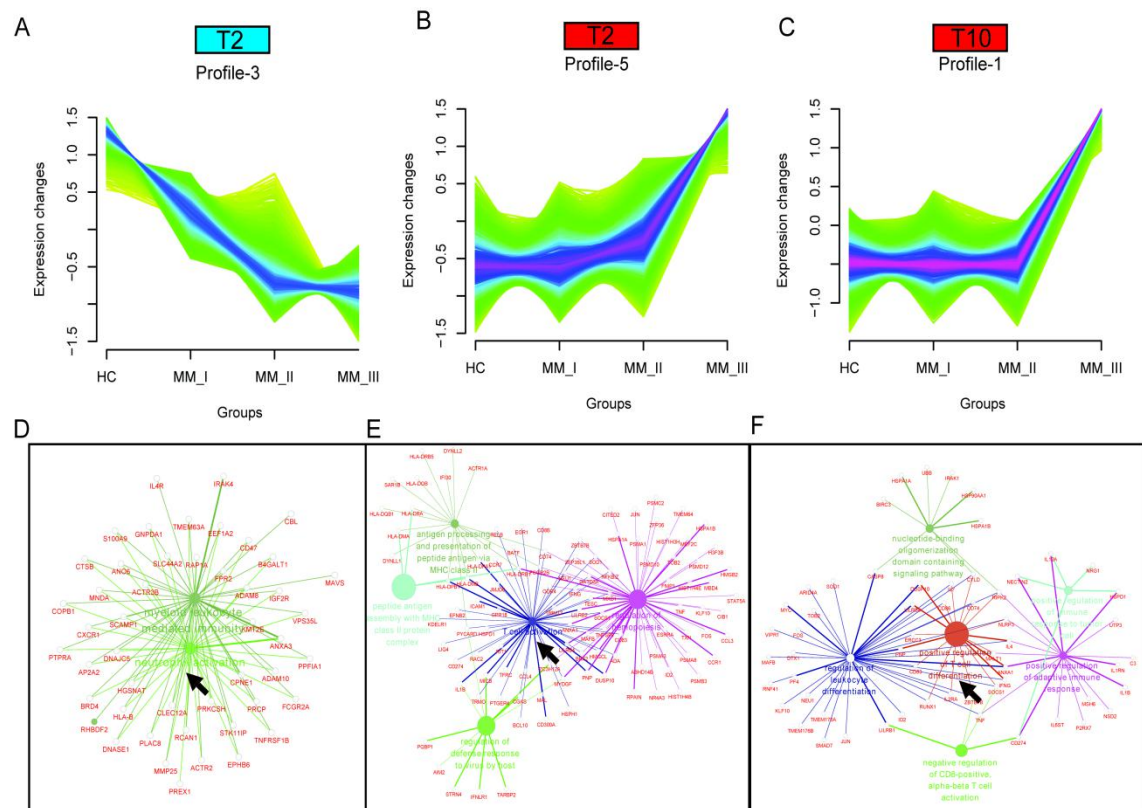
391 B) Based on markers expression in D ) CD4+T, CD8+T, NK and NKT cells were shown with  
392 UMAP;

393 C) UMAP of samples distribution of T cells and NK cells;

394 D) Markers of T cells and NK cells, shown with UMAP;

395 E) Cluster proportions in healthy control and MM groups;

396 F) Cluster proportions in healthy control, RISS-I, II and III MM groups.



397

398 **Figure7. Stage-dependent expression analysis reveals three gene modules in CD8+T and**  
 399 **NKT cell clusters.**

400 To acquire RISS stage dependent gene expression modules in Cluster 2 and 10 populations,  
 401 MFUZZ was acquired. Two gene profiles in Cluster2 (T2C3 and T2C5) and Cluster 10 (T10C1)  
 402 were generated.

403 A) Genes in T2C3 were generally characterized as gradually decreased expression with  
 404 stage;

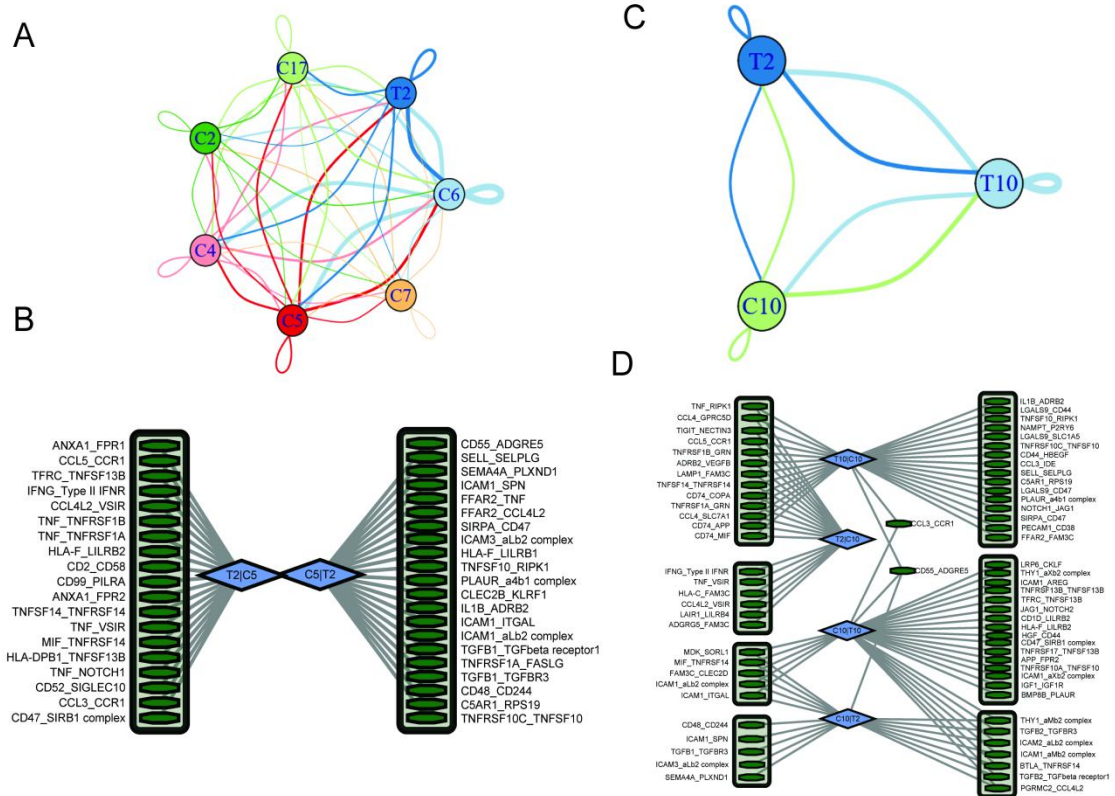
405 B) Genes in T2C5 were generally marked with stage dependent increased expression;

406 C) Genes in T10C1 were generally marked stable expression in healthy control, RISS I and II  
 407 stage, but remarkable elevation in III stage;

408 D) Functional network of genes in T2C3 highlights neutrophil activation of T2 cells;

409 E) Functional network of genes in T2C5 suggested genes in T cell activation;

410 F) Functional network of genes in T10C1 indicates genes in T cell differentiation.



411

412 **Figure8. Ligand-receptor pairs and potential immunotherapeutic targets in CD8+T-Neutrophil**  
413 **and CD8+T/NKT-plasma cells communication.**

414 A) Cell-cell communications showing the interaction numbers between myeloid cells and T2  
415 CD8+T cells;

416 B) Paracrine ligand-receptor interaction pairs between neutrophils and T2 CD8+T cells;

417 C) Cell-cell communications showing the interaction numbers between C10 plasma cells and  
418 T2 CD8+T cells, T10 NKT cells;

419 D) Paracrine ligand-receptor interaction pairs between C10 plasma cells and T2 CD8+T cells,  
420 T10 NKT cells;

421

422 **References**

- 423 1. Rajkumar, S.V., *Multiple myeloma: 2020 update on diagnosis, risk-stratification and*  
424 *management*. Am J Hematol, 2020. **95**(5): p. 548-567.
- 425 2. Palumbo, A., et al., *Revised International Staging System for Multiple Myeloma: A Report*  
426 *From International Myeloma Working Group*. J Clin Oncol, 2015. **33**(26): p. 2863-9.
- 427 3. Kastritis, E., et al., *Evaluation of the Revised International Staging System in an*  
428 *independent cohort of unselected patients with multiple myeloma*. Haematologica, 2017.  
429 **102**(3): p. 593-599.
- 430 4. Cho, H., et al., *Comprehensive evaluation of the revised international staging system in*  
431 *multiple myeloma patients treated with novel agents as a primary therapy*. Am J Hematol,  
432 2017. **92**(12): p. 1280-1286.
- 433 5. Galieni, P., et al., *The detection of circulating plasma cells may improve the Revised*  
434 *International Staging System (R-ISS) risk stratification of patients with newly diagnosed*  
435 *multiple myeloma*. Br J Haematol, 2021. **193**(3): p. 542-550.
- 436 6. Jung, S.H., et al., *(18)F-FDG PET/CT is useful for determining survival outcomes of*  
437 *patients with multiple myeloma classified as stage II and III with the Revised International*  
438 *Staging System*. Eur J Nucl Med Mol Imaging, 2019. **46**(1): p. 107-115.
- 439 7. Young, L.S., L.F. Yap, and P.G. Murray, *Epstein-Barr virus: more than 50 years old and still*  
440 *providing surprises*. Nat Rev Cancer, 2016. **16**(12): p. 789-802.
- 441 8. Wang, L.W., et al., *Epstein-Barr-Virus-Induced One-Carbon Metabolism Drives B Cell*  
442 *Transformation*. Cell Metab, 2019. **30**(3): p. 539-555 e11.
- 443 9. Xia, B., et al., *Epstein-Barr virus infection is associated with clinical characteristics and*  
444 *poor prognosis of multiple myeloma*. Biosci Rep, 2019. **39**(10).
- 445 10. Sperling, A.S. and K.C. Anderson, *Facts and Hopes in Multiple Myeloma Immunotherapy*.  
446 Clin Cancer Res, 2021.
- 447 11. Guillerey, C., et al., *Immune responses in multiple myeloma: role of the natural immune*  
448 *surveillance and potential of immunotherapies*. Cell Mol Life Sci, 2016. **73**(8): p. 1569-89.
- 449 12. Tremblay-LeMay, R., N. Rastgoo, and H. Chang, *Modulating PD-L1 expression in*  
450 *multiple myeloma: an alternative strategy to target the PD-1/PD-L1 pathway*. J Hematol  
451 Oncol, 2018. **11**(1): p. 46.
- 452 13. Minnie, S.A. and G.R. Hill, *Immunotherapy of multiple myeloma*. J Clin Invest, 2020.  
453 **130**(4): p. 1565-1575.
- 454 14. Nakamura, K., M.J. Smyth, and L. Martinet, *Cancer immunoediting and immune*  
455 *dysregulation in multiple myeloma*. Blood, 2020. **136**(24): p. 2731-2740.
- 456 15. Hofmeister, C.C. and S. Lonial, *How to Integrate Elotuzumab and Daratumumab Into*  
457 *Therapy for Multiple Myeloma*. J Clin Oncol, 2016. **34**(36): p. 4421-4430.
- 458 16. Ettari, R., et al., *Immunoproteasome-selective and non-selective inhibitors: A promising*  
459 *approach for the treatment of multiple myeloma*. Pharmacol Ther, 2018. **182**: p.  
460 176-192.
- 461 17. Yee, A.J., et al., *Ricolinostat plus lenalidomide, and dexamethasone in relapsed or*  
462 *refractory multiple myeloma: a multicentre phase 1b trial*. Lancet Oncol, 2016. **17**(11): p.  
463 1569-1578.
- 464 18. Dimopoulos, M.A., et al., *Current treatment landscape for relapsed and/or refractory*  
465 *multiple myeloma*. Nat Rev Clin Oncol, 2015. **12**(1): p. 42-54.

- 466 19. Ledergor, G., et al., *Single cell dissection of plasma cell heterogeneity in symptomatic*  
467 *and asymptomatic myeloma*. Nat Med, 2018. **24**(12): p. 1867-1876.
- 468 20. Lohr, J.G., et al., *Genetic interrogation of circulating multiple myeloma cells at single-cell*  
469 *resolution*. Sci Transl Med, 2016. **8**(363): p. 363ra147.
- 470 21. Jang, J.S., et al., *Molecular signatures of multiple myeloma progression through single*  
471 *cell RNA-Seq*. Blood Cancer J, 2019. **9**(1): p. 2.
- 472 22. Cohen, Y.C., et al., *Identification of resistance pathways and therapeutic targets in*  
473 *relapsed multiple myeloma patients through single-cell sequencing*. Nat Med, 2021.  
474 **27**(3): p. 491-503.
- 475 23. Zavidij, O., et al., *Single-cell RNA sequencing reveals compromised immune*  
476 *microenvironment in precursor stages of multiple myeloma*. Nat Cancer, 2020. **1**(5): p.  
477 493-506.
- 478 24. Ryu, D., et al., *Alterations in the Transcriptional Programs of Myeloma Cells and the*  
479 *Microenvironment during Extramedullary Progression Affect Proliferation and Immune*  
480 *Evasion*. Clin Cancer Res, 2020. **26**(4): p. 935-944.
- 481 25. Dutta, A.K., et al., *Subclonal evolution in disease progression from MGUS/SMM to*  
482 *multiple myeloma is characterised by clonal stability*. Leukemia, 2019. **33**(2): p. 457-468.
- 483 26. Anguiano, A., et al., *Gene expression profiles of tumor biology provide a novel approach*  
484 *to prognosis and may guide the selection of therapeutic targets in multiple myeloma*. J  
485 Clin Oncol, 2009. **27**(25): p. 4197-203.
- 486 27. Cupi, M.L., et al., *Plasma cells in the mucosa of patients with inflammatory bowel disease*  
487 *produce granzyme B and possess cytotoxic activities*. J Immunol, 2014. **192**(12): p.  
488 6083-91.
- 489 28. Neuse, C.J., et al., *Genome instability in multiple myeloma*. Leukemia, 2020. **34**(11): p.  
490 2887-2897.
- 491 29. Samur, M.K., et al., *Genome-Wide Somatic Alterations in Multiple Myeloma Reveal a*  
492 *Superior Outcome Group*. J Clin Oncol, 2020. **38**(27): p. 3107-3118.
- 493 30. Manier, S., et al., *Genomic complexity of multiple myeloma and its clinical implications*.  
494 Nat Rev Clin Oncol, 2017. **14**(2): p. 100-113.
- 495 31. Carrasco, D.R., et al., *The differentiation and stress response factor XBP-1 drives multiple*  
496 *myeloma pathogenesis*. Cancer Cell, 2007. **11**(4): p. 349-60.
- 497 32. Hideshima, T., et al., *p53-related protein kinase confers poor prognosis and represents a*  
498 *novel therapeutic target in multiple myeloma*. Blood, 2017. **129**(10): p. 1308-1319.
- 499 33. Rizq, O., et al., *Dual Inhibition of EZH2 and EZH1 Sensitizes PRC2-Dependent Tumors to*  
500 *Proteasome Inhibition*. Clin Cancer Res, 2017. **23**(16): p. 4817-4830.
- 501 34. Azab, A.K., et al., *Hypoxia promotes dissemination of multiple myeloma through*  
502 *acquisition of epithelial to mesenchymal transition-like features*. Blood, 2012. **119**(24): p.  
503 5782-94.
- 504 35. Gentles, A.J., et al., *The prognostic landscape of genes and infiltrating immune cells*  
505 *across human cancers*. Nat Med, 2015. **21**(8): p. 938-945.
- 506 36. Watanabe, T., et al., *Antitumor activity of cyclin-dependent kinase inhibitor*  
507 *alsterpaullone in Epstein-Barr virus-associated lymphoproliferative disorders*. Cancer Sci,  
508 2020. **111**(1): p. 279-287.
- 509 37. Yang, P.Y., et al., *Activity-based proteome profiling of potential cellular targets of*

- 510 *Orlistat--an FDA-approved drug with anti-tumor activities.* J Am Chem Soc, 2010. **132**(2):  
511 p. 656-66.
- 512 38. Molderings, G.J., et al., *Identification and pharmacological characterization of a specific*  
513 *agmatine transport system in human tumor cell lines.* Ann N Y Acad Sci, 2003. **1009**: p.  
514 75-81.
- 515 39. Nyce, J., *Drug-induced DNA hypermethylation and drug resistance in human tumors.*  
516 Cancer Res, 1989. **49**(21): p. 5829-36.
- 517 40. Chen, P., et al., *PI3K/Akt inhibitor LY294002 potentiates homoharringtonine antimyeloma*  
518 *activity in myeloma cells adhered to stromal cells and in SCID mouse xenograft.* Ann  
519 Hematol, 2018. **97**(5): p. 865-875.
- 520 41. Garcia-Ortiz, A., et al., *The Role of Tumor Microenvironment in Multiple Myeloma*  
521 *Development and Progression.* Cancers (Basel), 2021. **13**(2).
- 522 42. Kawano, Y., et al., *Targeting the bone marrow microenvironment in multiple myeloma.*  
523 Immunol Rev, 2015. **263**(1): p. 160-72.
- 524 43. Cohen, A.D., et al., *How to Train Your T Cells: Overcoming Immune Dysfunction in*  
525 *Multiple Myeloma.* Clin Cancer Res, 2020. **26**(7): p. 1541-1554.
- 526 44. Cohen, A.D., et al., *B cell maturation antigen-specific CAR T cells are clinically active in*  
527 *multiple myeloma.* J Clin Invest, 2019. **129**(6): p. 2210-2221.
- 528 45. Chim, C.S., et al., *Management of relapsed and refractory multiple myeloma: novel*  
529 *agents, antibodies, immunotherapies and beyond.* Leukemia, 2018. **32**(2): p. 252-262.
- 530 46. Kumar, L. and E.F. M, *Mfuzz: a software package for soft clustering of microarray data.*  
531 Bioinformatics, 2007. **2**(1): p. 5-7.
- 532 47. Ma, J.Z., et al., *METTL14 suppresses the metastatic potential of hepatocellular carcinoma*  
533 *by modulating N(6)-methyladenosine-dependent primary MicroRNA processing.*  
534 Hepatology, 2017. **65**(2): p. 529-543.
- 535 48. Chao, T., E.E. Furth, and R.H. Vonderheide, *CXCR2-Dependent Accumulation of*  
536 *Tumor-Associated Neutrophils Regulates T-cell Immunity in Pancreatic Ductal*  
537 *Adenocarcinoma.* Cancer Immunol Res, 2016. **4**(11): p. 968-982.
- 538 49. Nguyen-Jackson, H., et al., *STAT3 controls the neutrophil migratory response to CXCR2*  
539 *ligands by direct activation of G-CSF-induced CXCR2 expression and via modulation of*  
540 *CXCR2 signal transduction.* Blood, 2010. **115**(16): p. 3354-63.
- 541 50. Teijeira, A., et al., *CXCR1 and CXCR2 Chemokine Receptor Agonists Produced by Tumors*  
542 *Induce Neutrophil Extracellular Traps that Interfere with Immune Cytotoxicity.* Immunity,  
543 2020. **52**(5): p. 856-871 e8.
- 544 51. Pruessmeyer, J., et al., *Leukocytes require ADAM10 but not ADAM17 for their migration*  
545 *and inflammatory recruitment into the alveolar space.* Blood, 2014. **123**(26): p. 4077-88.
- 546 52. Treffers, L.W., et al., *IgA-Mediated Killing of Tumor Cells by Neutrophils Is Enhanced by*  
547 *CD47-SIRPalpha Checkpoint Inhibition.* Cancer Immunol Res, 2020. **8**(1): p. 120-130.
- 548 53. Efremova, M., et al., *CellPhoneDB: inferring cell-cell communication from combined*  
549 *expression of multi-subunit ligand-receptor complexes.* Nat Protoc, 2020. **15**(4): p.  
550 1484-1506.
- 551 54. D'Angiolella, V., et al., *Cyclin F-mediated degradation of ribonucleotide reductase M2*  
552 *controls genome integrity and DNA repair.* Cell, 2012. **149**(5): p. 1023-34.
- 553 55. Mazzu, Y.Z., et al., *A Novel Mechanism Driving Poor-Prognosis Prostate Cancer:*



- 554 *Overexpression of the DNA Repair Gene, Ribonucleotide Reductase Small Subunit M2*  
555 *(RRM2)*. Clin Cancer Res, 2019. **25**(14): p. 4480-4492.
- 556 56. Gandhi, M., et al., *The lncRNA lincNMR regulates nucleotide metabolism via a YBX1 -*  
557 *RRM2 axis in cancer*. Nat Commun, 2020. **11**(1): p. 3214.
- 558 57. Rahman, M.A., et al., *RRM2 regulates Bcl-2 in head and neck and lung cancers: a*  
559 *potential target for cancer therapy*. Clin Cancer Res, 2013. **19**(13): p. 3416-28.
- 560 58. Jones, R.J., et al., *HDM-2 inhibition suppresses expression of ribonucleotide reductase*  
561 *subunit M2, and synergistically enhances gemcitabine-induced cytotoxicity in mantle cell*  
562 *lymphoma*. Blood, 2011. **118**(15): p. 4140-9.
- 563 59. Pfister, S.X., et al., *Inhibiting WEE1 Selectively Kills Histone H3K36me3-Deficient Cancers*  
564 *by dNTP Starvation*. Cancer Cell, 2015. **28**(5): p. 557-568.
- 565 60. Liu, X., et al., *Silencing RRM2 inhibits multiple myeloma by targeting the Wnt/betacatenin*  
566 *signaling pathway*. Mol Med Rep, 2019. **20**(3): p. 2159-2166.
- 567 61. Jung, T.Y., et al., *Deacetylation by SIRT1 promotes the tumor-suppressive activity of*  
568 *HINT1 by enhancing its binding capacity for beta-catenin or MITF in colon cancer and*  
569 *melanoma cells*. Exp Mol Med, 2020. **52**(7): p. 1075-1089.
- 570 62. Motzik, A., et al., *Post-translational modification of HINT1 mediates activation of MITF*  
571 *transcriptional activity in human melanoma cells*. Oncogene, 2017. **36**(33): p. 4732-4738.
- 572 63. Wang, L., et al., *Hint1 inhibits growth and activator protein-1 activity in human colon*  
573 *cancer cells*. Cancer Res, 2007. **67**(10): p. 4700-8.
- 574 64. Gnanasundram, S.V., et al., *MDM2's dual mRNA binding domains co-ordinate its*  
575 *oncogenic and tumour suppressor activities*. Nucleic Acids Res, 2020. **48**(12): p.  
576 6775-6787.
- 577 65. Schmidt, S.C., et al., *Epstein-Barr virus nuclear antigen 3A partially coincides with*  
578 *EBNA3C genome-wide and is tethered to DNA through BATF complexes*. Proc Natl Acad  
579 Sci U S A, 2015. **112**(2): p. 554-9.
- 580 66. McIntosh, M.T., et al., *STAT3 imparts BRCAness by impairing homologous recombination*  
581 *repair in Epstein-Barr virus-transformed B lymphocytes*. PLoS Pathog, 2020. **16**(10): p.  
582 e1008849.
- 583 67. Bocchini, C.E., et al., *Protein stabilization improves STAT3 function in autosomal*  
584 *dominant hyper-IgE syndrome*. Blood, 2016. **128**(26): p. 3061-3072.
- 585 68. Barkal, A.A., et al., *CD24 signalling through macrophage Siglec-10 is a target for cancer*  
586 *immunotherapy*. Nature, 2019. **572**(7769): p. 392-396.
- 587 69. Veitonmaki, N., et al., *A human ICAM-1 antibody isolated by a function-first approach*  
588 *has potent macrophage-dependent antimyeloma activity in vivo*. Cancer Cell, 2013.  
589 **23**(4): p. 502-15.
- 590 70. Sherbenou, D.W., et al., *Potent Activity of an Anti-ICAM1 Antibody-Drug Conjugate*  
591 *against Multiple Myeloma*. Clin Cancer Res, 2020. **26**(22): p. 6028-6038.
- 592 71. Gu, W., et al., *CD44-Specific A6 Short Peptide Boosts Targetability and Anticancer*  
593 *Efficacy of Polymersomal Epirubicin to Orthotopic Human Multiple Myeloma*. Adv Mater,  
594 2019. **31**(46): p. e1904742.
- 595 72. Bjorklund, C.C., et al., *Evidence of a role for CD44 and cell adhesion in mediating*  
596 *resistance to lenalidomide in multiple myeloma: therapeutic implications*. Leukemia, 2014.  
597 **28**(2): p. 373-83.

- 598 73. Casucci, M., et al., *CD44v6-targeted T cells mediate potent antitumor effects against*  
599 *acute myeloid leukemia and multiple myeloma*. Blood, 2013. **122**(20): p. 3461-72.
- 600 74. Liu, D., *CAR-T "the living drugs", immune checkpoint inhibitors, and precision medicine:*  
601 *a new era of cancer therapy*. J Hematol Oncol, 2019. **12**(1): p. 113.
- 602 75. Hosen, N., et al., *CD48 as a novel molecular target for antibody therapy in multiple*  
603 *myeloma*. Br J Haematol, 2012. **156**(2): p. 213-24.
- 604 76. Burton, J.D., et al., *CD74 is expressed by multiple myeloma and is a promising target for*  
605 *therapy*. Clin Cancer Res, 2004. **10**(19): p. 6606-11.
- 606 77. Kaufman, J.L., et al., *Phase I, multicentre, dose-escalation trial of monotherapy with*  
607 *milatuzumab (humanized anti-CD74 monoclonal antibody) in relapsed or refractory*  
608 *multiple myeloma*. Br J Haematol, 2013. **163**(4): p. 478-86.
- 609 78. Zheng, Y., et al., *Role of Myeloma-Derived MIF in Myeloma Cell Adhesion to Bone*  
610 *Marrow and Chemotherapy Response*. J Natl Cancer Inst, 2016. **108**(11).
- 611 79. Sun, Y., et al., *Downregulation of LINC00958 inhibits proliferation, invasion and migration,*  
612 *and promotes apoptosis of colorectal cancer cells by targeting miR36195p*. Oncol Rep,  
613 2020. **44**(4): p. 1574-1582.
- 614 80. Guillerey, C., et al., *TIGIT immune checkpoint blockade restores CD8(+) T-cell immunity*  
615 *against multiple myeloma*. Blood, 2018. **132**(16): p. 1689-1694.
- 616 81. Lozano, E., et al., *Nectin-2 Expression on Malignant Plasma Cells Is Associated with Better*  
617 *Response to TIGIT Blockade in Multiple Myeloma*. Clin Cancer Res, 2020. **26**(17): p.  
618 4688-4698.
- 619 82. Minnie, S.A., et al., *Myeloma escape after stem cell transplantation is a consequence of*  
620 *T-cell exhaustion and is prevented by TIGIT blockade*. Blood, 2018. **132**(16): p.  
621 1675-1688.
- 622 83. Flores-Montero, J., et al., *Next Generation Flow for highly sensitive and standardized*  
623 *detection of minimal residual disease in multiple myeloma*. Leukemia, 2017. **31**(10): p.  
624 2094-2103.
- 625 84. Haghverdi, L., et al., *Batch effects in single-cell RNA-sequencing data are corrected by*  
626 *matching mutual nearest neighbors*. Nat Biotechnol, 2018. **36**(5): p. 421-427.
- 627 85. Macosko, Evan Z., et al., *Highly Parallel Genome-wide Expression Profiling of Individual*  
628 *Cells Using Nanoliter Droplets*. Cell, 2015. **161**(5): p. 1202-1214.
- 629 86. Aran, D., et al., *Reference-based analysis of lung single-cell sequencing reveals a*  
630 *transitional profibrotic macrophage*. Nature Immunology, 2019. **20**(2): p. 163-172.
- 631 87. Mabbott, N.A., et al., *An expression atlas of human primary cells: inference of gene*  
632 *function from coexpression networks*. BMC Genomics, 2013. **14**: p. 632.
- 633 88. Vogelstein, B., et al., *Cancer genome landscapes*. Science, 2013. **339**(6127): p. 1546-58.
- 634 89. Horst, A., et al., *Detection and characterization of plasma cells in peripheral blood:*  
635 *correlation of IgE+ plasma cell frequency with IgE serum titre*. Clin Exp Immunol, 2002.  
636 **130**(3): p. 370-8.
- 637 90. Livak, K.J. and T.D. Schmittgen, *Analysis of relative gene expression data using real-time*  
638 *quantitative PCR and the 2(-Delta Delta C(T)) Method*. Methods, 2001. **25**(4): p. 402-8.
- 639  
640

641 **Material and methods**

642 ***Patients and sample collection***

643 This study included 9 MM patients diagnosed as active MM according to International  
644 Myeloma Working Group guideline, and two age-matched normal control (transplant donor) .

645 For FACS analysis of MKI67 and PCNA in plasma cells, samples from 3 healthy donors, 5  
646 RISS-I, 4 R-ISS-II and 6 R-ISS III were collected. Written informed consents were obtained  
647 from all subjects. All experimental procedures were approved by the Institutional Review  
648 Board of Sichuan Provincial People's Hospital and carried out in accordance with the  
649 principles of the Declaration of Helsinki.

650 Bone marrow (BM) aspirates were collected into EDTA-containing tubes, and lysed using  
651 Versalyse Lysing Solution (cat. no. A09777; Beckman Coulter, Inc.). Mononuclear cells were  
652 isolated using a Ficoll gradient (density 1.077 g/ml, cat. no. 07801; STEMCELL Technologies).  
653 Fresh single-cell suspensions were used for ScRNA seq. Aliquots of the same bone biopsy  
654 were analyzed by fluorescence in situ hybridization (FISH) and multi-parameter flow cytometry  
655 (MFC, Navios Beckman Coulter, Inc.) as parts of the routine clinical diagnosis. In MFC, cell  
656 populations were considered abnormal if they have an atypical differentiation pattern, an  
657 increased or decreased expression level of normal antigens, an asynchronous maturational  
658 pattern or express aberrant antigens [83].

659 ***ScRNA-Seq library construction and sequencing***

660 Single-cell RNA-Seq libraries were prepared with Chromium Single cell 3' Reagent v3 Kits  
661 according to the manufacturer's protocol. Single-cell suspensions were loaded on the  
662 Chromium Single Cell Controller Instrument (10×Genomics) to generate single cell gel beads  
663 in emulsions (GEMs). Briefly, about  $2 \times 10^5$  PBMC single cells were suspended in calcium- and  
664 magnesium-free PBS containing 0.04% weight/volume BSA. About 22,000 cells were added to  
665 each channel with a targeted cell recovery estimate of 10,000 cells. After generation of GEMs,  
666 reverse transcription reactions were engaged barcoded full-length cDNA followed by the  
667 disruption of emulsions using the recovery agent and cDNA clean up with DynaBeads®

668 MyOne™ Silane Beads (Thermo Fisher Scientific). cDNA was then amplified by PCR with  
669 appropriate cycles which depend on the recovery cells. Subsequently, the amplified cDNA was  
670 fragmented, end-repaired, A-tailed, index adaptor ligated and library amplification. Then these  
671 libraries were sequenced on the Illumina sequencing platform (NovaSeq6000) and 150 bp  
672 paired-end reads were generated. The GEM generation, library construction and sequencing  
673 were performed by OE Biotech CO., LTD (Shanghai, China).

#### 674 ***ScRNA-Seq data processing***

675 The Cell Ranger software pipeline (version 3.1.0) provided by 10×Genomics was used to  
676 demultiplex cellular barcodes, map reads to the genome and transcriptome using the STAR  
677 aligner, and down-sample reads as required to generate normalized aggregate data across  
678 samples, producing a matrix of gene counts versus cells. We processed the unique molecular  
679 identifier (UMI) count matrix using the R package Seurat[84] (version 3.1.1). To remove low  
680 quality cells and likely multiplet captures, which is a major concern in microdroplet-based  
681 experiments, we applied criteria to filter out cells with UMI/gene numbers out of the limit of  
682 mean value  $\pm 2$  fold of standard deviations assuming a Guassian distribution of each cells'  
683 UMI/gene numbers. Following visual inspection of the distribution of cells by the fraction of  
684 mitochondrial genes expressed, we further discarded low-quality cells where >20% of the  
685 counts belonged to mitochondrial genes. After applying these QC criteria, 103043 single cells  
686 were retained for downstream analyses. Library size normalization was performed with  
687 Normalize Data function in Seurat[84] to obtain the normalized count. Specifically, the  
688 global-scaling normalization method “LogNormalize” normalized the gene expression  
689 measurements for each cell by the total expression, multiplied by a scaling factor (10,000 by  
690 default), and the results were logtransformed.

691 Top variable genes across single cells were identified using the method described in Macosko  
692 *et al*[85]. The most variable genes were selected using FindVariableGenes  
693 function(mean.function=ExpMean, dispersion.function= LogVMR) in Seurat[84]. To remove  
694 the batch effects in single-cell RNA-sequencing data, the mutual nearest neighbors (MNN)

695 presented by Haghverdi *et al*/ was performed with the R package batchelor[84]. Graph-based  
696 clustering was performed to cluster cells according to their gene expression profile using the  
697 FindClusters function in Seurat[84]. Cells were visualized using a 2-dimensional t-distributed  
698 stochastic neighbor embedding (t-SNE) algorithm with the RunTSNE function in Seurat[84].  
699 We used the FindAllMarkers function(test.use = bimod) in Seurat[84] to identify marker genes  
700 of each cluster. For a given cluster, FindAllMarkers identified positive markers compared with  
701 all other cells. Then, we used the R package SingleR[86], a novel computational method for  
702 unbiased cell type recognition of scRNA-seq, with the reference transcriptomic datasets  
703 'Human Primary Cell Atlas'[87] to infer the cell of origin of each of the single cells  
704 independently and identify cell types.

705 Differentially expressed genes (DEGs) were identified using the FindMarkers function (test.use  
706 = MAST) in Seurat[84]. P value < 0.05 and  $|\log_2\text{foldchange}| > 0.58$  was set as the threshold for  
707 significantly differential expression. GO enrichment and KEGG pathway enrichment analysis  
708 of DEGs were respectively performed using R based on the hypergeometric distribution.

#### 709 ***Large-scale chromosomal copy number variation analysis***

710 The normalized scRNA-seq gene expression matrices were used to estimate CNV profiles  
711 with inferCNV R package[88]. Genes were sorted based on their chromosomal location and a  
712 moving average of gene expression was calculated using a window size of 101 genes. The  
713 expression was then centered to zero by subtracting the mean. The de-noising was carried out  
714 to generate the final CNV profiles.

#### 715 ***Cell cycle analysis***

716 Cell cycle genes were defined as those with a "cell cycle process" Gene Ontology annotation  
717 (downloaded from MSigDB version 3.1). We defined four cell cycle signatures (G1/S, S, G2/M,  
718 and M) as the average expression  $[\log_2(\text{TPM} + 1)]$  of phase-specific subsets of the cell cycle  
719 genes. We refined these signatures by averaging only over those genes whose expression  
720 pattern in our data correlated highly ( $r > 0.5$ ) with the average signature of the respective cell  
721 cycle phase (before excluding any gene) in order to remove the influence of genes.

722 ***Cell culture***

723 Human normal plasma cells were separated from the peripheral blood of healthy donors using  
724 flow cytometry. All donors were healthy volunteers who had not previously received any drugs  
725 associated with immunological diseases. Briefly, peripheral blood mononuclear cells were  
726 separated by Ficoll®-Hypaque centrifugation from peripheral blood. Plasma cells were  
727 isolated from mononuclear blood cells using CD138 microbeads (Miltenyi Biotec, Inc.)  
728 according to the manufacturer's instructions [89]. The isolated plasma cells were then cultured.  
729 The U266 and MM1.S cell lines were purchased from the American Type Culture Collection.  
730 RPMI-1640 medium (Gibco; Thermo Fisher Scientific, Inc.) containing 10% fetal bovine serum  
731 (Gibco; Thermo Fisher Scientific, Inc.) and 1% dual antibiotics (penicillin 100 U/ml;  
732 streptomycin 0.1 mg/ml; Sigma-Aldrich; Merck KGaA) was used to culture all cells at 37°C  
733 with 5% CO<sub>2</sub>.

734 ***RRM2 and HINT1 silencing with shRNAs***

735 Short hairpin RNAs specifically targeting RRM2 and HINT1 were designed and synthesized by.  
736 RRM2 shRNAs were shRNA1 (5'-3'): GGAGCGATTTAGCCAAGAA , shRNA2 (5'-3'):  
737 GCCTCACATTTTCTAATGA and shRNA3 (5'-3'): GAAAGACTAACTTCTTTGA. HINT1  
738 shRNAs were: shRNA1 (5'-3'): GGTGGTGAATGAAGTTCA , shRNA2 (5'-3'):  
739 GTGATACCCAAGAAACATA and shRNA3 (5'-3'): GTCTGTCTATCACGTTTCAT.

740 The shRNAs were cloned into pcDNA3.1, and transfected into the MM cells. Transfection was  
741 performed according to the manufacturer's protocol using Lipofectamine® 3000 reagent.  
742 Following co-culture for 12 h at 37°C, the medium was replaced with culture media and the  
743 transfected cells were used for subsequent experiments. Forty-eight hours post transfection,  
744 RRM2 and HINT1 expression in the cells was determined by reverse transcription quantitative  
745 polymerase chain reaction (RT-qPCR), and the transfection efficiency was verified.

746 ***RNA extraction and reverse transcription-quantitative RT-qPCR***

747 Total RNA from cells was extracted using TRIzol (Invitrogen; Thermo Fisher Scientific, Inc.).  
748 cDNA was synthesized using the PrimeScript RT reagent kit (Takara Biotechnology Co., Ltd.)  
749 at 25°C for 5 min, 37°C for 30 min and 85°C for 5 sec. qPCR analysis was performed using the

750 StepOnePlus Real-Time PCR system (Applied Biosystems; Thermo Fisher Scientific, Inc.)  
751 with SYBR Premix EX Taq kit (Takara Biotechnology Co., Ltd.). Primer sequences for RRM2,  
752 HINT1 were as following: RRM2 Forward 5'-3': CCAATGAGCTTCACAGGCAA, Reverse 5'-3':  
753 TGGCTCAAGAAACGAGGACT. HINT1 Forward 5'-3': TTGCCGACCTCCAAGAACAT, Reverse  
754 5'-3': CCCTCAAGCACCAACACATT. Relative expression was calculated using the  $2^{-\Delta\Delta Cq}$   
755 method [90].

#### 756 ***CCK8 assays for cell proliferation***

757 Cell proliferation assay was performed with Cell Counting Kit-8 (Dojindo, Kumamoto, Japan)  
758 according to the manufacturer's instruction. Twenty-four hour after transfection, cells were  
759 seed in 96-well plates at  $1 \times 10^4$  U266 cells per well. The proliferative ability of U266 cells was  
760 determined at 0, 24 and 48 h. The absorbance was measured at 450 nm using a microplate  
761 spectrophotometer (Molecular Devices, Sunnyvale, USA).

#### 762 ***Statistical analysis***

763 Statistical analysis and graph representations were performed using SPSS v.13.0 software  
764 (SPSS Inc., Chicago, IL) and GraphPad Prism 8 Software (GraphPad, San Diego, CA),  
765 respectively. One-way ANOVA with post hoc Tukey's test was used to compare differences  
766 between multiple groups. For cell assays, data are presented as the mean  $\pm$  standard deviation  
767 (SD) and were compared using either Student's *t* test or the Mann-Whitney *U* test. The  
768 Kaplan-Meier method was used for survival analyses.  $P < 0.05$  was considered statistically  
769 significant.

770